MASSACHUSETTS INSTITUTE OF TECHNOLOGY
ARTIFICIAL INTELLIGENCE LABORATORY

and

CENTER FOR BIOLOGICAL INFORMATION PROCESSING
WHITAKER COLLEGE

A.I. Memo 790
C.B.I.P. Paper 007

July, 1984

Kinematic Features of Unrestrained Arm Movements

Christopher G. Atkeson & John M. Hollerbach

Abstract.

Unrestrained human arm trajectories between point targets have been investigated using a three dimensional tracking apparatus, the Selspot system. Movements were executed between different points in a vertical plane under varying conditions of speed and hand-held load. In contrast to past results which emphasized the straightness of hand paths, movement regions were discovered in which the hand paths were curved. All movements, whether curved or straight, showed an invariant tangential velocity profile when normalized for speed and distance. The velocity profile invariance with speed and load is interpreted in terms of simplification of the underlying arm dynamics, extending the results of Hollerbach and Flash (1982).

This report describes research done within the Artificial Intelligence Laboratory and the Center for Biological Information Processing (Whitaker College) at the Massachusetts Institute of Technology. Support for the A. I. Laboratory's research in artificial intelligence is provided in part by the Advanced Research Projects Agency of the Department of Defense under Office of Naval Research contract N00014-80-C-0505. The Center's support is provided in part by the Sloan Foundation and in part by the Whitaker College. Additional support was provided by NIH Research Grant AM 26710, awarded by the National Institute of Arthritis, Metabolism, and Digestive Diseases, and by an NSF Graduate Fellowship (CGA).

1. Introduction

We have investigated unrestrained human arm trajectories between point targets using a three dimensional tracking apparatus, the Selspot system. Our studies indicate the importance of examining natural unrestricted movements, as our results agree only in part with previous studies of arm movement. Past observations on multi-joint human arm trajectories obtained from restricted horizontal planar movements measured with a gripped pantograph have shown in both humans and monkeys that point to point trajectories are essentially straight with bell-shaped velocity profiles (Morasso, 1981; Abend, Bizzi, and Morasso, 1982). Moreover, they satisfy a time scaling property that may be related to the underlying dynamics (Hollerbach and Flash, 1982). We sought to corroborate these observations for more natural unrestricted arm movements and also to examine the effects of different loads and of gravity on the arm trajectories.

A strategy for gaining insight into planning and control processes of the motor system is to look for kinematic invariances in trajectories of movement. The significance of straight-line movements of the hand during arm trajectories is that they imply movement planning at the hand or object level (Morasso, 1981; Hollerbach, 1982), that is to say, in terms of coordinates or variables that are external to the biological system and that could be matched to tasks or outside constraints. One alternative to object-level planning is that movements are planned at the joint level, that is, in terms of joint angles and their time evolution independent of considerations of what the hand is doing except for beginning and end points. The simplest example of joint-level planning is joint-interpolated motion, where each joint angle is interpolated from beginning joint position to final joint position under the same time function (see e.g. Taylor, 1979). Evidence for joint-level planning is apparently provided in a series of papers examining unrestrained vertical arm movement (Soechting and Lacquaniti, 1981; Lacquaniti and Soechting, 1982; Lacquaniti, Soechting, and Terzuolo, 1982), where it is proposed that the ratio of joint angle rates of shoulder and elbow is maintained constant in the last part of a trajectory. This amounts to joint-level planning because a constant joint rate ratio can be shown to be formally equivalent to joint interpolation (Hollerbach and Atkeson, 1984).

Although one would expect on the basis of kinematics alone that joint-level motion planning would not lead to straight-line hand movements, the data presented by these researchers seem to show both straight-line hand movements and constant joint rate ratio. This apparently contradictory situation has nevertheless been recently resolved as an artifact of kinematics and workspace (Hollerbach and Atkeson, 1984), because as movements approach the workspace boundary the joint rate ratio approaches a constant value. More recently, Soechting and Lacquaniti (1983) have proposed synergies in the shoulder muscle EMG, which would represent planning at a level below the joint level, the actuator level (Hollerbach, 1982). The actuator level here means planning in terms of individual muscle activations, which differs from joint-level planning because of the redundant musculature around a joint and multi-joint muscle action.

While subjects seem to produce voluntarily straight-line motions in point-to-point reaching movements, it is certainly the case that subjects can generate curved trajectories at will or in response to task requirements. In two-dimensional movement, examples include of course handwriting (Hollerbach, 1981), obstacle avoidance or via point intersection (Abend, Bizzi, and Morasso, 1982), or self-initiated curved motions (Viviani and Terzuolo, 1982). In three-dimensional movement, examples include response to change of target location during movement (Soechting and Lacquaniti, 1983) and self-initiated curved motions (Morasso, 1983). As with straight-line movement, the planning of curved movements has been explained at the various levels of hand, joint, and actuator.

In addition to path curvature, there has been a focus on the time function along a path, that is to say, the shape of the tangential velocity profile. For single-joint elbow movement, Hogan (1984) proposed that the measured bell-shaped velocity profiles could

be described by a minimum-jerk cost function. Nelson (1983) investigated a number of optimization criteria that could be used to derive velocity profiles, and deduced among other things that for repetitive movement a minimum-jerk strategy is almost indistinguishable from a mass-spring model. Meyer, Smith, and Wright (1982) considered speed-accuracy tradeoffs in proposing an acceleration profile which is notable for a double inflection point from acceleration to deceleration. For two-joint arm movement, a number of researchers have noted a bell-shaped velocity profile essentially similar to the single-joint case (Morasso, 1981; Abend, Bizzi, and Morasso, 1982). Flash (1983) showed that the two-joint case could also be modeled by a minimum jerk strategy, and that in fact the two-joint curved movements (Abend, Bizzi, and Morasso, 1982) could be modeled by jerk minimization as well.

While velocity profile characteristics may be taken as evidence of end-point trajectory planning strategies, Hollerbach and Flash (1982) have proposed that an invariant velocity profile shape for a given path may represent a simplifying strategy for movement speed modification. If movement speed along a fixed path is varied by stretching or compressing the velocity profile uniformly, then in principle the joint torques for the new movement speed are simply related to the old joint torques. This method of torque formation requires separate treatment of the gravity torques and the dynamic or drive torques, which are proportional to joint acceleration and product of joint velocities. In demonstrating the possibility of speed scaling, Hollerbach and Flash (1982) examined only horizontal planar arm movements due to apparatus restrictions. Since gravity does not act in the horizontal plane of movement, a better test of speed scaling and the proposed separate treatment of gravity and drive torques is to investigate movement in a vertical plane where gravity is a factor.

Recently we have developed the capability of measuring unrestricted vertical or any other movements with a Selspot system, and this paper reports in part on results concerning speed scaling for vertical arm movements. Additionally we examine load effects on trajectory, where weights are held in a subject's hand. Lacquaniti, Soechting, and Terzuolo (1982) report that trajectory is unaffected by load. Before embarking on the hand load experiments, we had expected that the joint torques would change in a complex manner when the load was changed. Thus our expectation was that path regularity and velocity profile invariance might break down, but the results caused us to reanalyze the analytic complexity of joint torque formation under conditions of varying load.

2. Methods

2.1. Experimental Procedures

2.1.1. Experimental Conditions

Human subjects sat in a chair in the viewing area of a three dimensional tracking system, the Selspot system (SELCOM), with infrared light emitting diodes (LEDs) attached to their right arm. The subjects were told that they would be moving their arms between two target zones indicated by visible light emitting diode targets (Fig. 1). These target diodes were mounted on the tip of dowels attached to an adjacent pegboard wall. The target zones were defined by showing the subjects the current pair of visible LED targets and asking the subjects to move the tip of their first finger to a point which was about an inch to the right of the activated target LED. Five subjects were used in this study, two male and three female, in the age range of 25-40.

The movement trials were conducted under the following conditions. There was no visual feedback of the current arm position. There was no light in the room except for the target LED which did not illuminate a large volume and was turned off under computer control as the subject's finger approached the destination target zone. There was also

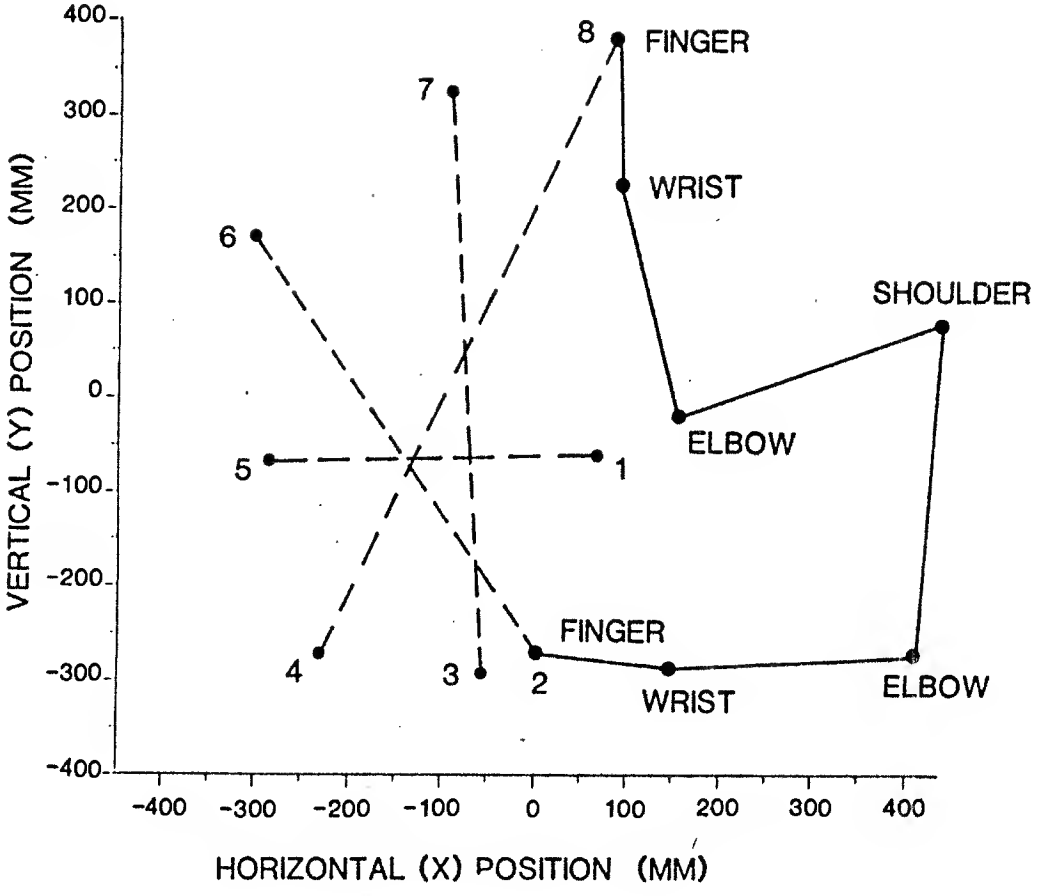

Figure 1 Location of Targets and Subject: the four pairs of targets used in this study are numbered 1-5, 2-6, 3-7, and 4-8. The locations of the targets shown here are approximate in that we adjusted the target locations for each subject to insure that the targets were well within the subject's reach. The XY projections of the segments of a typical subject's arm are indicated in two configurations by the solid lines. Because the subject's elbow was often out of the XY plane by varying amounts the lengths of the solid lines do not indicate the true arm segment lengths but only the lengths of their XY projections.

no tactile feedback as no target was touched at any time. The subjects were told not to worry about the fine accuracy of the movement and were discouraged from making corrective movements after the initial movement ended. No instruction was given about path or trajectory execution. In trials with an external load the load was held by the subjects in their hand during the movement. Only the two targets currently in use were in place during the movement trials so that there were no obstacles in the movement area.

2.1.2. Experimental Protocol

After being familiarized with the location of the target zones and the target sequence for a pair of targets the subjects executed the following sequence of trials with no external load:

(i) Six trials in which the speed instruction was "Move slowly between the targets." The average duration of these movements was 1200 msec.

(ii) Six trials in which the speed instruction was "Move at your normal speed." The average duration of these movements was 800 msec.

(iii) Ten trials in which the speed instruction was "Move as fast as you can." The average duration of these movements was 400 msec.

This sequence of trials was then repeated with two different external loads (two of 2, 3, or 4 lbs. depending on subject strength). After this the pair of targets was changed and the entire sequence repeated with a new pair of targets.

A movement trial consisted of:

(i) Auditory cue.

(ii) The start target LED was turned on and the subject aligned himself in the start target zone.

(iii) The start target LED was turned off and sampling was started.

(iv) 240 milliseconds later the destination target LED was turned on. Occasionally subjects started moving before the destination target was illuminated. Starting sampling 240 milliseconds before turning on the target allowed these early movements to be collected.

(v) The subject moved to the destination target zone.

(vi) As the subject's finger approached this target zone the destination target LED was turned off, leaving the subject in darkness.

(vii) The subject completed the movement.

In the following trial the roles of the targets were reversed with the former destination target being the start target and the former start target being the destination target. For six trials between two targets A and B there are three movements from A to B interspersed with three movements from B to A (A to B, B to A, A to B, ...). This entire protocol was executed under computer control.

2.1.3. Attaching Selspot Markers

The infrared LED markers were placed on the subject so as to facilitate later reconstruction of the subject's elbow and shoulder angles (to be presented in a subsequent paper). LED 1 was placed at the end of the subject's pointing finger. Two metal strips were prepared with an infrared marker at each end and attached to the subject's upper arm and forearm aligned with the axis of each body segment (Fig. 2). By measuring the 3-dimensional position of each strip end the orientation of the strip in space can be obtained. The forearm strip had one end placed over the wrist to mark its approximate location.

2.1.4. Data Aquisition

The Selspot system in combination with a computer (PDP11/34) was used to measure the position in three dimensions of the infared marker LEDs on the subject's arm. The X and Y position of each LED as viewed from two Selspot cameras placed at approximately 90° to each other was recorded every 3.17 msec (315 Hz). Digital LED positions were acquired via a direct memory access interface (DR11B) and stored concurrently on a computer disk. Due to the high data rate of the Selspot system the duration of sampling was controlled by the subject's movement. The subject's finger's arrival in the target zone was detected and used to turn off sampling a certain number of samples later. (A similar scheme was used to turn off the target LED as the subject's finger approached it.) The number of samples taken after the end of the movement depended on the expected movement speed ranging from 315 (1 sec) for a fast movement to 630 (2 sec) for a slow movement.

Due to the large amounts of data collected and the limited disk space available the data were packed. The Selspot system we used provides 10 bits of data for each measurement. By subtracting subsequent measurements each data point was stored in 4 bits as a difference. Differences larger than ±7 were handled specially as were Selspot bad

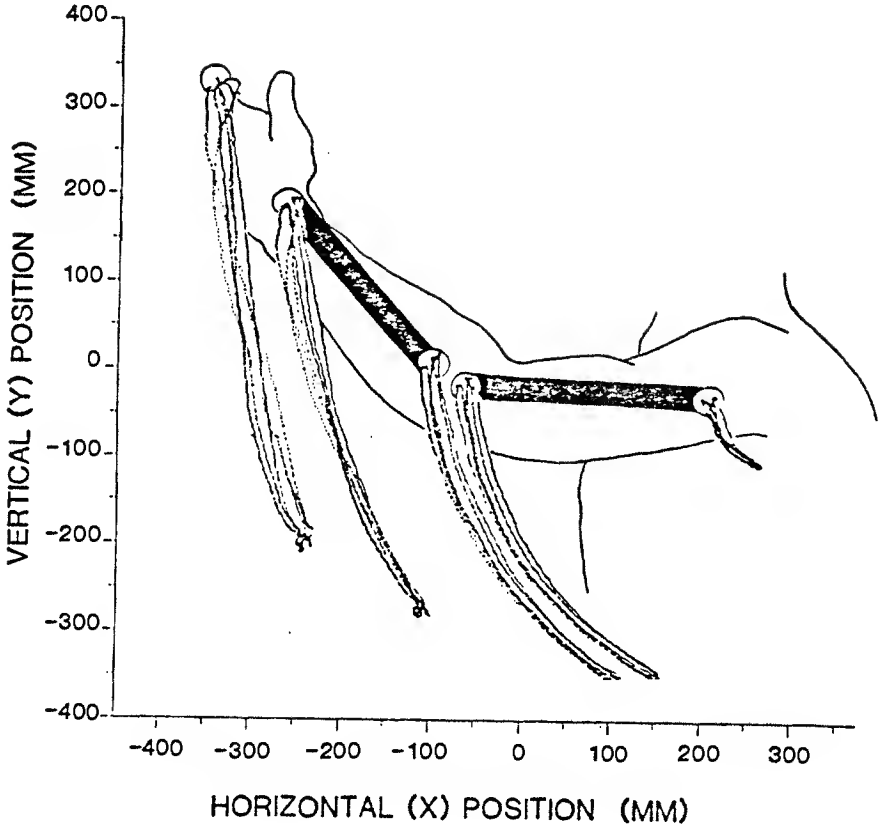

Figure 2 Attachment of Selspot Markers and Data Presentation: locations of the Selspot infrared LED markers and the typical format of the data presentation. Note that the wrist and one of the elbow LEDs are connected by a rigid bar aligned with the forearm, and the shoulder and other elbow LEDs are similarly connected on a rigid bar aligned with the upper arm. The three dimensional Selspot data is projected onto the XY plane. This projection shows most of the features of the path because these movements were almost planar (for the finger, wrist, and shoulder) and oriented parallel to the XY plane. In each data plot several movements are presented. Three upward movements (dotted lines) are indicated here by a dot at the location of the infrared LED for each sample (sampling frequency 315 Hz). Three downward movements are indicated by solid lines marking the path of each infrared LED.

data points. This nibble difference packing scheme was used to reduce the size of data and the rate at which data had to be written to disk. During later processing the data were reconstructed exactly with no loss of information.

2.2. Data Processing

The data were later processed off line to obtain the three dimensional positions for the LED markers, joint angles, and other parameters of interest. The software for data processing

evolved from previously developed algorithms (Conati, 1977; Tetewski, 1978). Currently our software is substantially different from other Selspot software, although we have incorporated some aspects of recent developments from Antonsson (1978), Antonsson (1982), and Reece (1981).

2.2.1. Obtaining Marker LED Three Dimensional Coordinates

The raw data from the Selspot system is in the format of an X and Y coordinate from each of two cameras for each LED in each sample. The first stage of data processing is unpacking the raw data. Several goals are achieved in this first module.

(i) The data is unpacked from 4 bit nibbles into 16 bit integers.

(ii) The data is offset and the Y axis reversed so that the lens center is at (0, 0) and a conventional coordinate system is used.

(iii) The data is reorganized in a convenient form for later filtering. Data from a single coordinate from a single LED are collected and stored in one record.

(iv) The start and end of the movement are detected by examining the raw data for changes in measured LED positions. This information is used to later trim the data so that large portions at the beginning and end of the trial that have no movements are removed.

The next stage of data processing is filtering the raw data. The filtering method used is to convolve the data with a finite impulse response designed to have the appropriate filtering characteristics (pass band: 0-6 Hz, transition band: 6-24 Hz, stop band: 24-∞ Hz) (McClellan, Parks, and Rabiner, 1973). This digital filtering method allows the use of filters with no phase lag to minimize distortion of the movement. Several steps are required to filter the data.

(i) Data points in which an LED was out of view are marked as bad.

(ii) Data points in which reflections of the infrared beam and other noise caused a spurious reading are detected by using a regression to find points that deviate from their neighbors by more than a certain threshold. These points are also marked as bad.

(iii) Bad points are filled in using a mixture of linear interpolation and cubic splines and the ends of the data record are extrapolated to allow all of the data to be convolved with the fixed length (63 points) finite impulse response filter. At this point the ends of the data are trimmed so that only the movement and a surrounding border of 50 points before the start of the movement and 150 points after the end of the movement are processed and stored in later stages.

(iv) The data is now convolved with the finite impulse response filter.

(v) Filled in points are removed from the filtered data.

The finite impulse response filter also includes a gain coefficient so that 16 bits are obtained from the 10 bit Selspot data. All filter calculations are done in double integer precision (32 bits).

The filtered data is now corrected using a lookup table for each camera coordinate. These tables were produced by putting LED markers in known positions relative to each camera and recording the average measured positions. Deviations between the expected measurement and the actual measurement were calculated and corrections for these deviations were mapped into a 25 by 25 lookup table. Standard interpolation techniques were used to calculate the table originally and to read corrections from the table.

Three dimensional positions of the LEDs are now calculated from the corrected data using the known positions and orientations of the cameras and geometry. Points for which the vectors to the reconstructed LED position from each camera origin miss by greater than a certain threshold (3 cm) are marked as bad. The Selspot system in our configuration can

detect movements of the markers as small as 1mm. Currently the absolute accuracy of the system is within ± 1 cm.

Once again the data is packed to conserve storage space. Each 16 bit integer is reduced to 4 bits by taking the third difference (the discrete analog of the third derivative or jerk). The discrete jerk was empirically determined to require the least number of bits to store. The data can be reconstructed completely with no loss of information for further analysis.

2.2.2. Normalization of Tangential Velocity Profiles

In the Results, it will be noted that the shape of the tangential velocity profile of the wrist LED is invariant. That is to say, if trajectories are normalized for time and distance and then aligned they should exactly coincide for different movements. To illustrate the normalization procedure, define

$v(t)$ as the experimental tangential velocity profile as a function of time t,

v_{max} as the maximum tangential velocity in $v(t)$,

d as the experimental movement distance,

v_{ref} as the reference velocity, and

d_{ref} as the reference distance.

The reference velocity and distance are chosen arbitrarily, and all data records are scaled to them. Since the tangential velocity profiles $v(t)$ are almost always unimodal, the maximum tangential velocity v_{max} is well defined. We use v_{max} rather than movement duration because of imprecision in determining movement start and stop points. Now define time and distance scaling factors c and a as

$$c = \frac{v_{ref}}{v_{max}}$$
$$a = \frac{d_{ref}}{d}$$

The velocity profile $v'(t)$ normalized first for distance is

$$v'(t) = a\,v(t)$$

The maximum velocity for the new velocity profile is then $v'_{max} = a\,v_{max}$. Define a new time scaling factor $c' = v_{ref}/v'_{max} = c/a$. Then the time-normalized velocity profile $v''(t)$ is

$$\begin{aligned} v''(t) &= c'v'(c't) \\ &= c\,v\left(\frac{c}{a}t\right) \end{aligned}$$

An example of the results of normalization is given in Fig. 3, where Fig. 3A contains the tangential velocity profiles before normalization and Fig. 3B after normalization.

2.3. A Note on Terminology

Two features of a movement are discussed in this paper, the path and the trajectory. The path of the arm is the curve in space traced out by the tip of the arm. The trajectory of the arm is the path of the arm and the time history of the tip of the arm along that curve in space. In the current study we present results mainly for the path and trajectory of the wrist LED. The derivation and analysis of joint angles are the subject of a future study.

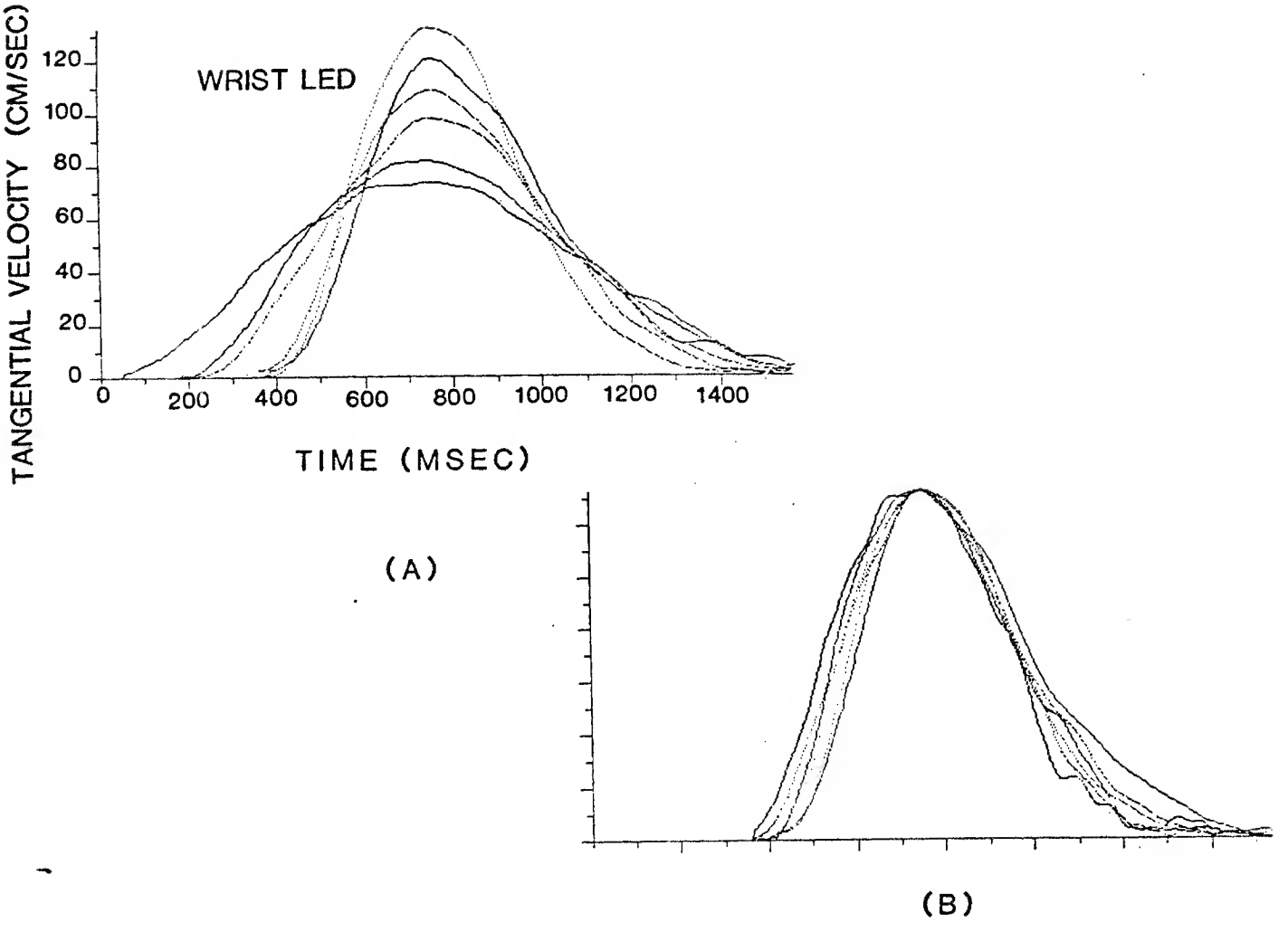

Figure 3 Normalization of Tangential Velocity Profiles: (A) a set of typical tangential velocity profiles of the wrist LED, derived from six unloaded movements at slow speeds between targets 3 and 7. (B) Normalized tangential velocity profiles when the effect of the different speeds has been divided out. Notice that the peak tangential velocities are now all the same and that the time axis has been compressed by the appropriate factor $(\frac{v_{ref}}{v_{max}})$ for each profile. That the normalized tangential velocity profiles have the same shape (and are therefore invariant) is indicated by their substantial overlap. The units for the normalized tangential velocity profile have no physical meaning and are therefore not indicated.

3. Results

3.1. Path Curvature and Workspace

Results obtained from previous planar two joint horizontal arm movement studies suggest that the wrist paths tend to be straight lines (Abend, Bizzi, and Morraso, 1982; Hollerbach and Flash, 1982; Georgopoulos, Kalaska, and Massey, 1981; Morasso, 1981). In contrast, we have observed curved as well as straight movements where the amount of curvature is dependent on the workspace. Substantially straight paths were observed for movements between targets 1-5 and 2-6 (Fig. 4A and 4B), whereas vertical movements between targets

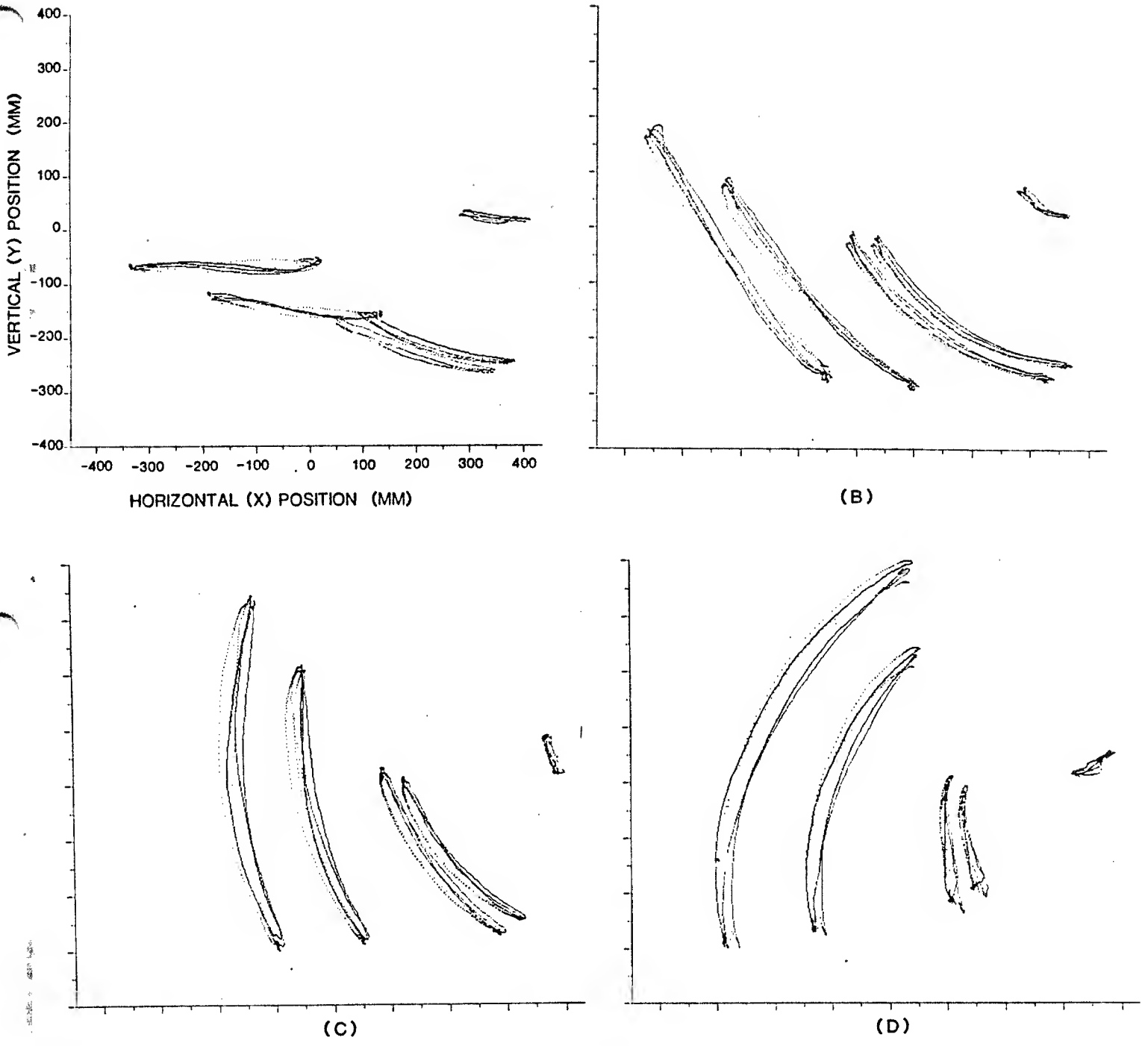

Figure 4 Typical Arm Trajectories: one subject's medium speed unloaded trajectories between each pair of targets: (A) 1-5, (B) 2-6, (C) 3-7, (D) 4-8. In (B-D) upward movements are dotted lines, downward movements are solid lines; in (A) movements to the left are dotted while movements to the right are solid lines. In (A-B) the wrist and finger movement paths are approximately straight while in (C-D) the wrist and finger paths are curved.

3-7 (Fig. 4C) and particularly movements between targets 4-8 (Fig. 4D) were curved.

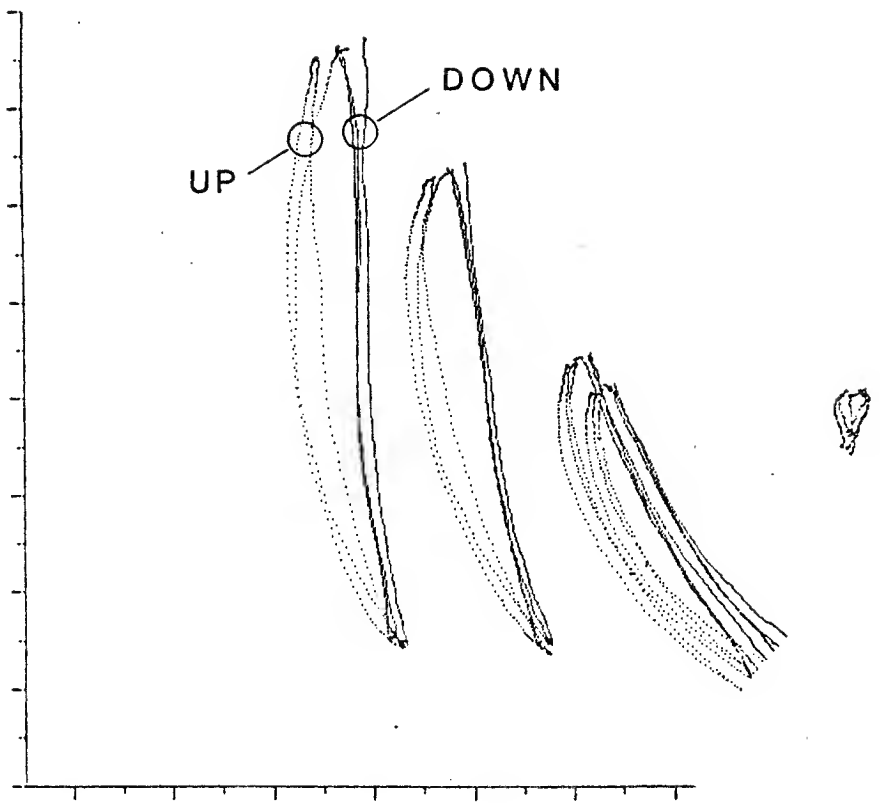

Figure 5 Path Dependence on Direction: one subject's normal speed unloaded trajectories between targets 3 and 7 show a dependence on movement direction. Upward movements are dotted while downward movements are solid lines. These movements are grouped according to their direction and do not overlap.

While these results represent a normal-speed motion without weights for one subject, they generalize to other subjects and to other speed/weight conditions.

For two of the five subjects there were marked asymmetries in the paths for upward versus downward movements (Fig. 5). This path dependence on direction has not been observed in previous experiments. Horizontal planar arm movements recorded in previous experiments are almost always straight lines, and therefore there can be little dependence of curvature on movement direction as there is little curvature. Previous studies of vertical movements did not compare movements in opposite directions (Lacquaniti and Soechting, 1982; Soechting and Lacquaniti, 1981); moreover, their movement directions only corresponded to those which in our studies also showed straight line trajectories.

3.2. Small Practice Effect

The regularity of the observed trajectories was not greatly influenced by practice. Fig. 6 shows an unloaded slow movement between targets 4-8 that was executed for the first

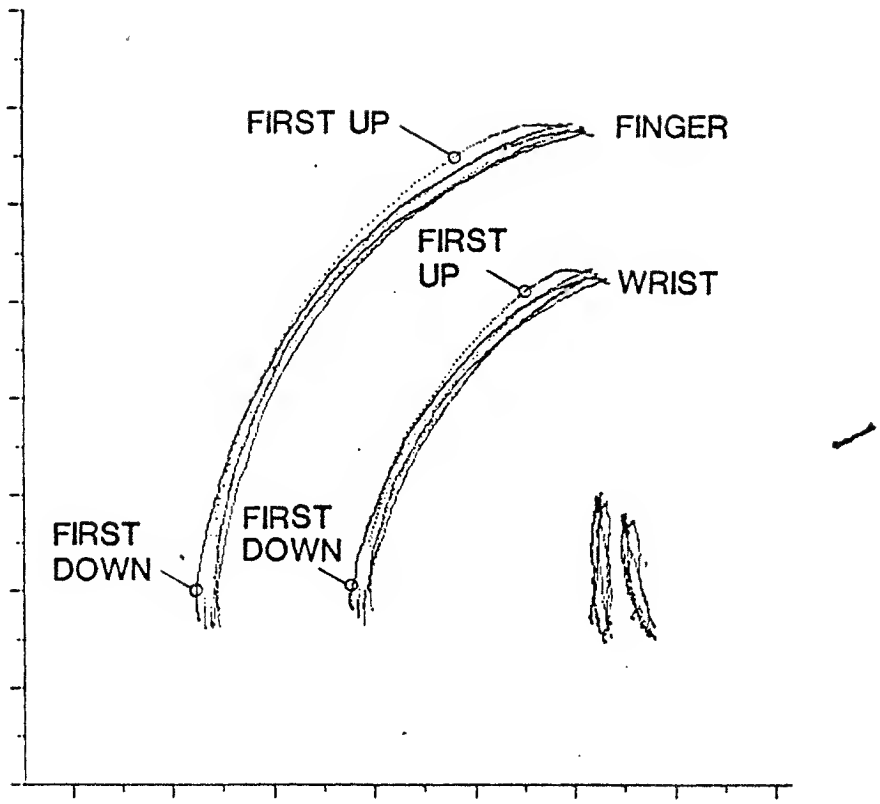

Figure 6 Small Practice Effect: slow unloaded trajectories between targets 4 and 8 are the first trajectories executed by this subject between these targets. The only trend in these trajectories is the change in the end point of the trajectory due to the subject's changing location of the final target. The first trajectories executed upwards and downwards are indicated.

time. The first movement in each direction is distinguished only by the error made by the subject in locating the target, Otherwise they are kinematically very similar to the following trajectories. The absence of a practice effect may be due to the low spatiotemporal accuracy constraints imposed on the subjects.

3.3. Path Invariance with Speed and Load

The path through space is invariant with movement speed and with load weight. Path invariance with movement speed is illustrated in Fig. 7, which represents overplots of movements between targets 3 and 7 at slow, normal, and fast speeds. It can be seen that the trajectory of the wrist point, which is more regular than the trajectory of the finger point, is similar for the different movement speed conditions. This observation holds for paths in other parts of the workspace as well.

Load weight invariance is illustrated in Fig. 8, representing overplots of the wrist path

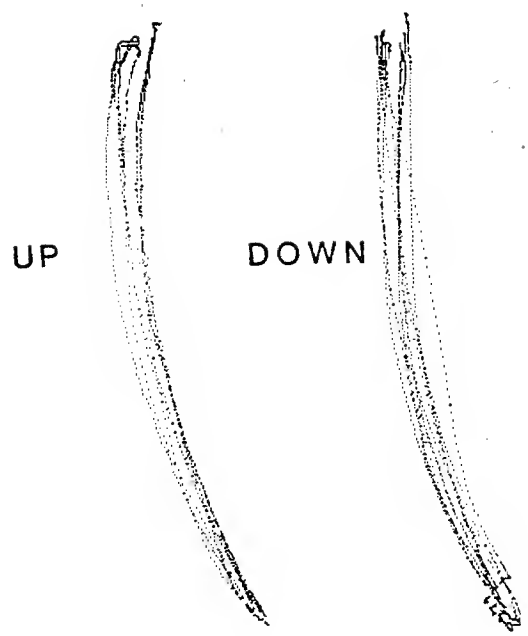

Figure 7 Path Invariance Across Different Speeds: one subject's unloaded wrist trajectories between targets 3 and 7 are compared for six slow movements (three upward and three downward), six medium, and six fast. Upward wrist movements are superimposed on the left, downward wrist movements on the right. Movements in the same direction overlap substantially; individual trajectories show no trend in changes of the paths with increased speed.

between targets 3-7 for a medium-speed unloaded, 2-pound loaded, and a 4-pound loaded movement. Again, this invariance holds throughout the workspace as well as at different movement speeds.

3.4. Scaling of the Tangential Velocity Profile

The shape of the tangential velocity profile remains invariant, when normalized according to the procedure of section 1.2.2, across movement speeds, load conditions, paths, and even subjects. Vertical movements for one subject are compared at slow, normal, and fast speeds without load in Fig. 9; tangential velocities for the downward movements have been made negative to distinguish them from the upward movements. The tangential velocity profiles are seen to substantially overlap. Scaling of movement speed was first observed in (Hollerbach and Flash, 1982) for restricted horizontal planar arm movements.

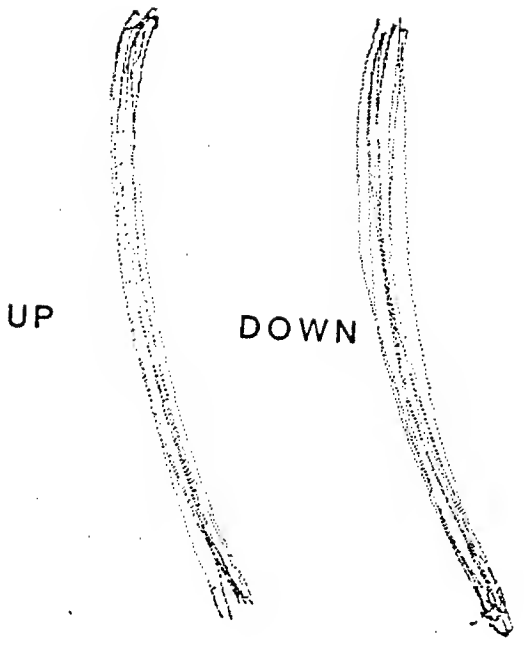

Figure 8 Path Invariance Across Different Loads: medium speed trajectories of the wrist for one subject between targets 3 and 7 are compared for 6 unloaded movements (again three upward and three downward), 6 with 2 lb hand-held load, and six with 4 lb hand-held load. Upward movements are superimposed on the left, downward movements on the right. The paths are similar, and examination of individual trajectories showed no grouping on the basis of the load condition.

Tangential velocity profiles also remain invariant with load. Fig. 10 shows a comparison of scaled velocity profiles for normal speed vertical movements with no load and with 4 pounds. The load scaling invariance holds for other movement speeds and across movement speeds.

Even when different paths are compared, the tangential velocity profiles are similar. Normal speed, unloaded movements were compared among the 4 different target pairs; Fig. 11 shows the similarity of the scaled tangential velocity profiles. As compared to the previous two figures, here in particular the profiles must be scaled for movement distance.

Most surprisingly, when movements from different subjects are compared, the velocity profiles remain invariantly shaped. Three different subjects executing unloaded movements between targets 3 and 7, two at a normal speed and in contrast one at fast speed, have been compared in Fig. 12, where again the tangential velocity profiles have been normalized

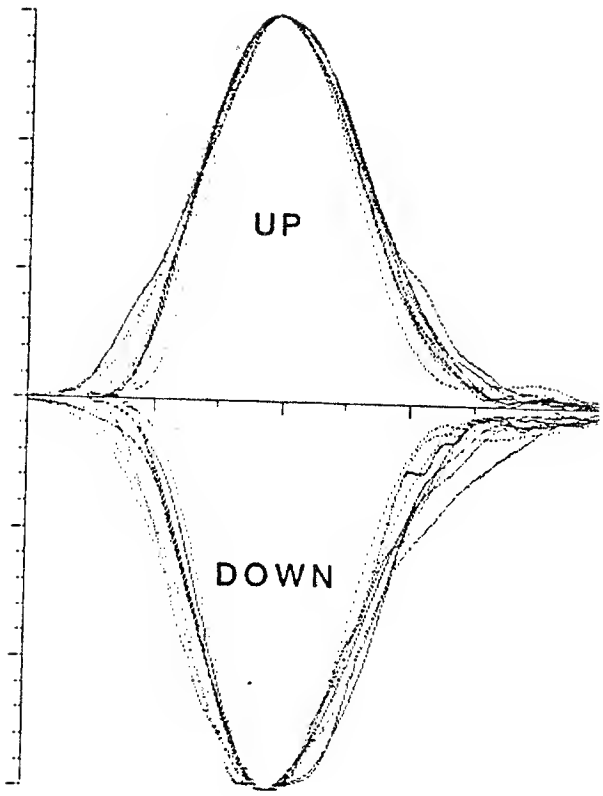

Figure 9 Tangential Velocity Profile Shape Invariance Across Different Speeds: illustrated by normalized tangential velocity profiles for one subject's unloaded movements between targets 3 and 7 at slow, medium, and fast speeds. Downward movements are plotted as having negative tangential velocities so they can be distinguished from the upward movements. Slow and fast movements are dotted here while medium speed movements are presented as solid lines. These profiles all overlap indicating that the same shape tangential velocity profile was executed in each case.

for distance and time.

4. Discussion

Taken together, path invariance and tangential profile shape invariance indicate that subjects execute only one form of trajectory between any two targets when not instructed to do otherwise. The only changes in the trajectory are simple scaling operations to accomodate different speeds. Furthermore, subjects use the same tangential velocity profile shape to make radically different movements even when the shapes of the paths are not the same in extrinsic coordinates. Different subjects use the same tangential velocity profile shape. These are unexpected results and raise many questions. The fact that the invariances still

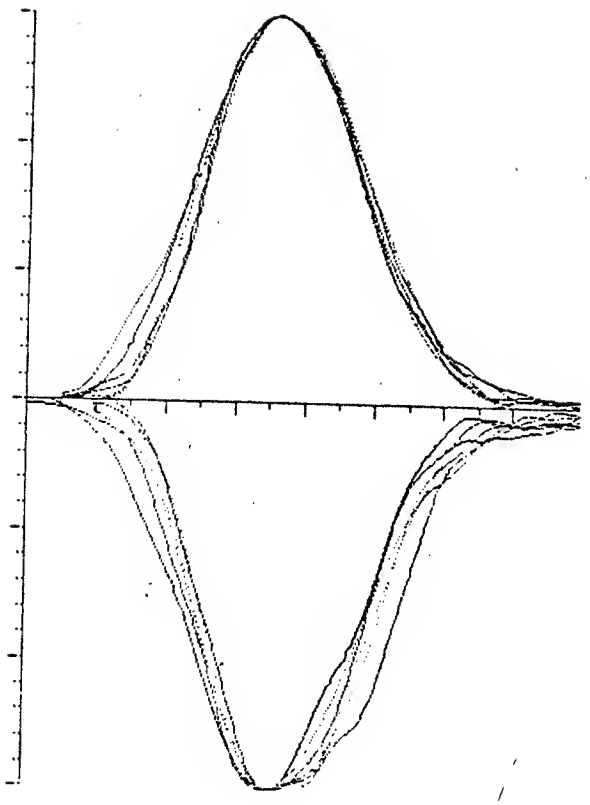

Figure 10 Tangential Velocity Profile Shape Invariance Across Different Loads: illustrated by normalized tangential velocity profiles from one subject's medium-speed movements between targets 3 and 7 executed under different load conditions. Unloaded movements are shown as dotted lines, loaded movements with a 4 lb hand-held load as solid lines. Again there is an almost complete overlap of the normalized tangential velocity profiles indicating that loads had no effect on the shape of the trajectory.

occur when subjects are asked to move as fast as possible indicates the importance of these invariances. We expected muscle constraints, which are extremely dependent on arm configuration and therefore location of the movement in the reachable area, to dominate in the fast movements. This did not happen. In the following discussion we will try to account for these findings. Because of the tangential velocity profile shape invariance across different movements and subjects we feel that issues of path and tangential velocity generation can be dealt with separately.

4.1. Path Shape

The dependence of path curvature on the movement start and end points is a new and surprising result. Past studies have emphasized the approximate linearity of arm endpoint trajectories, primarily in horizontal planar movements where the degrees of freedom of motion

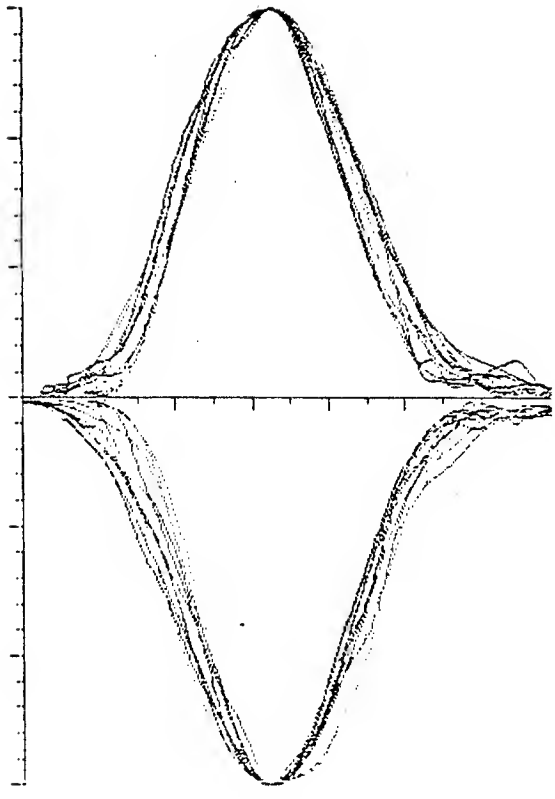

Figure 11 Tangential Velocity Profile Shape Invariance Across Different Movements: illustrated by normalized tangential velocity profiles from one subject's medium-speed unloaded movements between all target pairs. Movements between targets 1-5 and 3-7 are shown as dotted lines, movements between targets 2-6 and 4-8 as solid lines. These profiles cannot be distinguished.

were limited to two by the pantograph measurement apparatus (Morasso, 1981; Abend, Bizzi, and Morasso, 1982; Hollerbach and Flash, 1982). Other studies in vertical-plane, unrestricted arm movements also showed straight line trajectories (Soechting and Lacquaniti, 1981; Lacquaniti and Soechting, 1982; Lacquaniti, Soechting, and Terzuolo, 1982), but the movement regions studied were similar to those regions in our studies where the trajectories are also seen to be straight.

There are three major differences between the present experiments and those involving the horizontal planar arm experiments, all of which could to some extent account for the curvature in our study. First, gravity acts in the vertical planar movements but not in the horizontal planar movements. Thus the curvature could result, for example, from difficulties in handling gravity in certain directions, or from energy considerations. In two subjects in particular, the effects of gravity were most notable because the upward movements were curved and the downward movements were fairly straight. Relative to the other subjects,

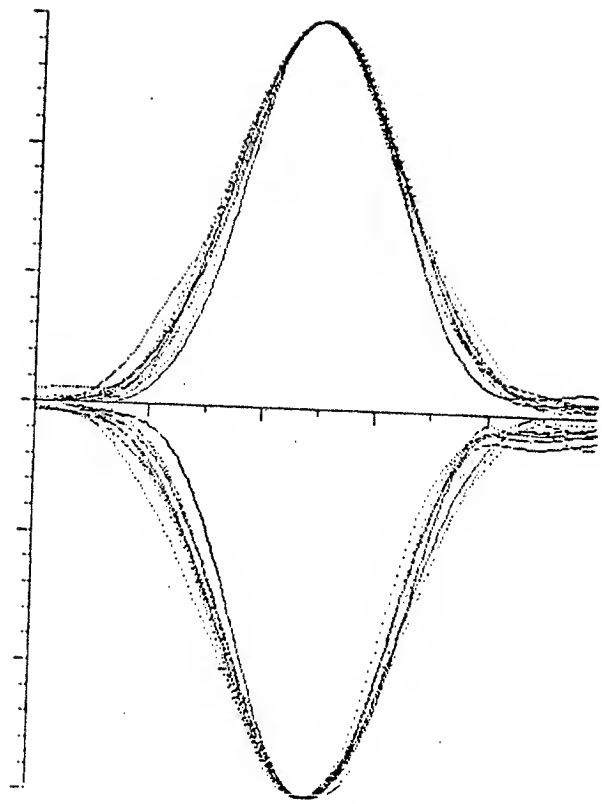

Figure 12 Tangential Velocity Profile Shape Invariance Across Subjects: illustrated by normalized tangential velocity profiles for fast speed unloaded movements between targets 3 and 7 from three subjects. Once again we see the same bell shaped tangential velocity profile in all cases. Movements of the same subject as presented in Figs. 9-11 are shown as solid lines, movements of the other two subjects as dotted lines.

these subjects had weak arm strengths. The upward curvature could represent a strategy to compensate for force production ability, while the downward linearity could represent a dropping of the arm to take advantage of, rather than fight, gravity.

Second, the vertical movements are in some sense more natural than the horizontal movements, since people seldom make the kinds of horizontal movements required by the apparatus. Third, the restricted degrees of freedom in the horizontal movements places these movements into the class of compliant motions (Brady, Hollerbach, Johnson, Lozano-Perez, and Mason, 1982), rather than into the class of free arm trajectories as in the present studies. A compliant motion is defined as any trajectory in which the hand motions are constrained by external contact; in the directions of the contact only forces can be generated and not displacements. At least in robotics, compliant motions are executed under a different control strategy than free motions, so that perhaps the compliant horizontal movements are also fashioned with a different control strategy. In vertical movements it would be as if

the motions had to be in contact with a vertical wall the whole time. We plan to conduct experiments to ascertain more precisely where the different experimental results arise from.

We do not yet have a full explanation for why certain movements are curved while others are straight. Preliminary analysis indicates that the vertical movements are generated by movement of the shoulder joint only, so that naturally the hand trajectories are curved. For the upward and diagonally inward curved motion between targets 4 and 8, both the elbow and shoulder joints seem to be moving. Hollerbach and Atkeson (1984) have shown that joint-interpolated motions lead to well-defined curved motions, but whether the target 4-8 movements can be explained in terms of joint interpolation is not yet known. In terms of tangential velocity profile invariance, it can be shown that for a single-joint movement the tangential velocity profile exactly mirrors the joint velocity profile. For a curving movement where both joints are active, however, the tangential and joint velocity profiles are not simply related. In the latter case, the invariances in the tangential velocity profiles seem to suggest that even though the paths are curved, a hand-based strategy is in effect.

4.2. Dynamic Scaling Properties for Speed and Load

A partial explanation for the velocity profile invariances with speed and load may be provided by an examination of arm movement dynamics. Hollerbach and Flash (1982) suggested that movement speed could be simply scaled if the joint torques due to gravity $\underline{\tau}^{arm}_{gravity}$ are separated from the joint torques arising from the acceleration and velocity product terms $\underline{\tau}^{arm}_{drive}$. Then the total joint torques $\underline{\tau}$ are (Appendix A)

$$\underline{\tau}(t) = \underline{\tau}^{arm}_{drive}(t) + \underline{\tau}^{arm}_{gravity}(t), \tag{1}$$

where the superscript *arm* is introduced now to distinguish the analysis of load dynamics later. If the movement is sped up or slowed down by a factor c, the new joint torques $\tilde{\underline{\tau}}$ are related to the old by

$$\tilde{\underline{\tau}}(t) = c^2 \underline{\tau}^{arm}_{drive}(ct) + \underline{\tau}^{arm}_{gravity}(ct). \tag{2}$$

The amplitudes of the drive torques scale by c^2 while the gravity torque amplitudes remain unchanged, which is the reason for the separation of joint torques into two components. Thus the new movement dynamics are simply obtained from the old.

To understand the effect of load on the underlying dynamics, we hypothesize a phantom arm that carries the load at the tip and mimics the movement of the actual arm (Fig. 13). This phantom arm has massless links and the same link lengths as the actual arm. Again, the phantom arm joint torques $\underline{\tau}^{load}$, where the superscript *load* is used to indicate torques associated with the phantom arm, are divided into drive and gravity components.

$$\underline{\tau}^{load} = \underline{\tau}^{load}_{drive} + \underline{\tau}^{load}_{gravity}. \tag{3}$$

If the load mass scales by r, and under the assumption that the load moment of inertia scales by r as well, the new phantom arm torques $\tilde{\underline{\tau}}^{load}$ are (Appendix B)

$$\tilde{\underline{\tau}}^{load} = r\,\underline{\tau}^{load}_{drive} + r\,\underline{\tau}^{load}_{gravity}. \tag{4}$$

If speed scaling by a factor c is included as well, then from (B16)

$$\tilde{\underline{\tau}}^{load} = c^2 r\,\underline{\tau}^{load}_{drive} + r\,\underline{\tau}^{load}_{gravity}. \tag{5}$$

The phantom arm torques are combined with the actual arm torques to indicate how the joint torques vary with speed and load.

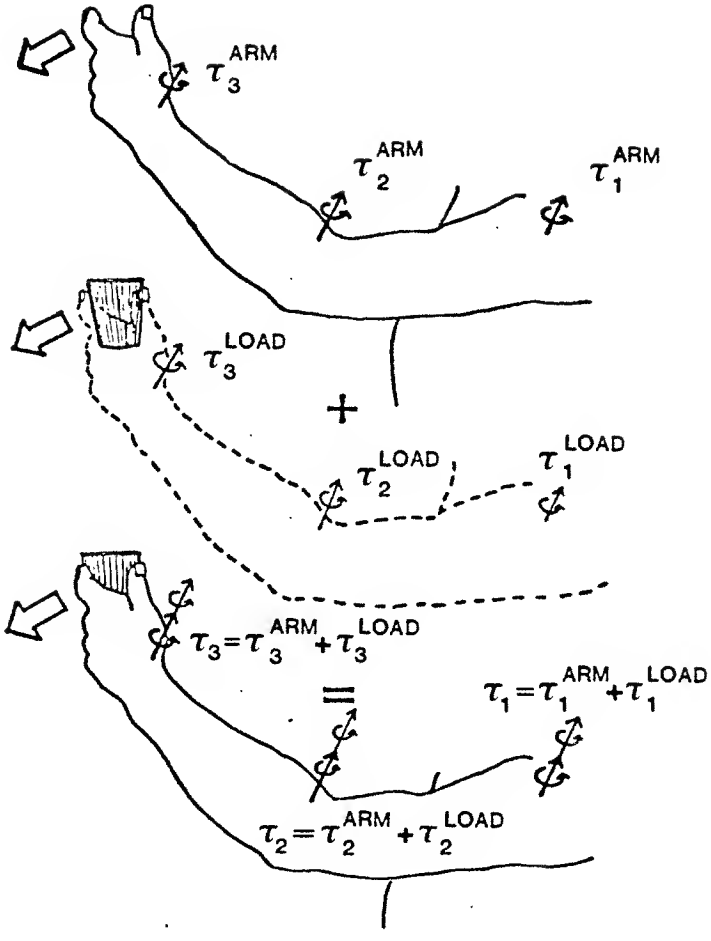

Figure 13 Separation of Arm Dynamics and Load Dynamics Computation: For any movement the torques necessary to drive the arm ($\underline{\tau}^{arm}$) without the load (top arm) can be combined with the torques necessary to drive the load. The load torques ($\underline{\tau}^{load}$) can be found by examining a phantom arm (dotted arm) that mimics the geometrical structure of the actual arm but is massless so it requires no torques to drive it. The phantom arm does require torques ($\underline{\tau}^{load}$) to drive the load it holds at the tip. The total torques necessary to drive the arm plus the load are the sum of ($\underline{\tau}^{load}$) and ($\underline{\tau}^{arm}$) (bottom arm).

$$\tilde{\underline{\tau}} = c^2\,\underline{\tau}^{arm}_{drive} + \underline{\tau}^{arm}_{gravity} + c^2 r\,\underline{\tau}^{load}_{drive} + r\,\underline{\tau}^{load}_{gravity}. \qquad (6)$$

The dynamics for the new movement are obtained by simple linear combination of dynamic components of the old movement.

In principle, therefore, it is not difficult for a motor controller to change movement speed and load, provided that the velocity profile is kept the same. If the velocity profile shape were changed, then the movement dynamics would change differently and would have to be refashioned in a more complex manner. This result says nothing about what the shape of the velocity profile for a given movement between two points should be (Flash, 1983), only that once chosen the motor controller should retain it under speed and load

changes. This result also does not require that movements between different points have the same velocity profile.

A number of issues remain with regard to these dynamic scaling results. How are the initial torques for the first instance of a movement generated? If the motor controller has the ability to fashion the correct torques for one movement, why does it not use this same ability for all subsequent movements rather than utilize the dynamic scaling properties? Among the possibilities we are considering, the first is a generalized motor tape where only one movement between points need be known if the dynamic components in (4) are stored separately. A motor tape for each possible start and finish point would be required, however, which renders this concept still unattractive. A second possibility is a modification of tabular approaches (Raibert, 1978), where the dimensionality and parameter adjustment problems could be reduced by separate tables for the 4 components in (4). The problem of how the tables are adapted for new, sudden loads is now solved, and the higher velocity and acceleration dimensions of the tables could be eliminated because slower movements could be scaled up. The resulting table sizes still required are however not clear.

Further experiments are suggested by the assumptions about the linear scaling of the load moments of inertias. We would predict that there would be some trajectory deviation if the load inertia scaling departs substantially from linearity from trial to trial. It should be mentioned that a complete proof of trajectory scaling would require the comparison of accelerations as well as of velocities, because similarly shaped velocity profiles might have fairly different acceleration profiles. The accuracy of our data does not currently warrant the calculation of accelerations, although future development of our measurement system will strive for improved accuracy. For the more accurate measurements of horizontal movements with the planar pantograph, the acceleration and torque scaling were seen to hold reasonably well (Hollerbach and Flash, 1982).

5. Summary

1. The observations of these trajectories tightly corroborate the previous horizontal results for velocity profile and time scaling but not for path straightness.

2. Path curvature or straightness depends on the location of target points in the workspace. For vertical movements, upward and downward movements between the same pairs of targets are sometimes different.

3. Different speed conditions and different hand-held loads do not significantly change the path of the movement; most often, the path is unchanged.

4. The time scaling property of movements holds not only across speeds but also across different hand-held loads, different pairs of targets, and different subjects.

5. The time scaling of arm dynamics with changes in speed and load suggest an explanation for the strong time invariance of human movement.

6. Acknowledgments

We would like to acknowledge early contributions of Michael Propp and Jonathan Delatizky towards development of our Selspot system, and of Eric Saund for display software development.

7. References

Abend, W., Bizzi, E., and Morasso, P. (1982) Human arm trajectory formation. Brain 105: 331-348.

Andriacchi, T. P., Hampton, S. J., Schultz, A. B., and Galante, J. O. (1979) Three-dimensional coordinate data processing in human motion analysis. J. Biomech. Eng. 101: 279-283.

Antonsson, E. K. (1978) The derivation and implementation of a dynamic three-dimensional linkage analysis technique. S. M. Thesis, Department of Mechanical Engineering, Massachusetts Institute of Technology.

Antonsson, E. K. (1982) A three-dimensional kinematic acquisition and intersegmental dynamic analysis system for human motion. Ph. D. Thesis, Department of Mechanical Engineering, Massachusetts Institute of Technology.

Brady, J. M., Hollerbach, J. M., Johnson, T. L., Lozano-Perez, T., and Mason, M. T., eds. (1982) Robot Motion: Planning and Control. MIT Press, Cambridge, Mass..

Conati, F. C. (1977) Real-time measurement of three-dimensional multiple rigid body motion. S. M. Thesis, Department of Mechanical Engineering, Massachusetts Institute of Technology.

Flash, T. (1983) Organizing principles underlying the formation of hand trajectories. Ph. D. Thesis, Harvard/MIT Division of Health Sciences and Technology.

Georgopoulos, A. P., Kalaska, J. F., and Massey, J. T. (1981) Spatial trajectories and reaction times of aimed movements: effects of practice, uncertainty, and change in target location. J. Neurophysiol. 46: 725-743.

Hogan, N. (1984) An organizing principle for a class of voluntary movements. J. Neuroscience : submitted.

Hollerbach, J. M. (1981) An oscillation theory of handwriting. Biol. Cybern. 39: 139-156.

Hollerbach, J. M. (1982) Computers, brains, and the control of movement. Trends in Neurosci. 5 no. 6: 189-192.

Hollerbach, J. M. (1984) Dynamic scaling of manipulator trajectories. ASME J. Dynamic Systems, Meas., Control 106: 102-106.

Hollerbach, J. M., and Atkeson, C. G. (1984) Characterization of joint-interpolated arm movements. Abst. 14th Neuroscience, Anaheim, California..

Hollerbach, J. M., and Flash, T. (1982) Dynamic interactions between limb segments during planar arm movement. Biol. Cybern. 44: 67-77.

Lacquaniti, F., and Soechting, J. F. (1982) Coordination of arm and wrist motion during a reaching task. J. Neurosci. 2: 399-408.

Lacquaniti, F., Soechting, J. F., and Terzuolo, C. A. (1982) Some factors pertinent to the organization and control of arm movements. Brain Res. 252: 394-397.

McClellan, J. H., Parks, T. W., and Rabiner, L. R. (1973) A computer program for designing optimum FIR linear phase digital filters. IEEE Trans. Audio Electroacoust. AU-21: 506-526.

Meyer, D., Smith, J. E. K., and Wright, C. (1982) Models for the speed and accuracy of aimed movements. Psych. Review 89: 449-482.

Morasso, P. (1981) Spatial control of arm movements. Exp. Brain Res. 42: 223-227.

Morasso, P. (1983) Three dimensional arm trajectories. Biol. Cybern. 48: 1-8.

Nelson, W. (1983) Physical principles for economies of skilled movements. Biol. Cybern. 46: 135-147.

Raibert, M. H. (1978) A model for sensorimotor control and learning. Biol. Cybern. 29: 29-36.

Reece, D. A. (1981) A Selspot-based data acquisition system for use in a clinical motion study laboratory. M. S. Thesis, Department of Electrical Engineering and Applied Physics, Case Western Reserve.

Soechting, J. F., and Lacquaniti, F. (1981) Invariant characteristics of a pointing movement in man. J. Neurosci. 1: 710-720.

Soechting, J. F., and Lacquaniti, F. (1983) Modification of trajectory of a pointing movement in response to a change in target location. J. Neurophysiol. 49: 548-564.

Taylor, R. H. (1979) Planning and execution of straight-line manipulator trajectories. IBM J. Res. Develop. 23: 424-436.

Tetewsky, A. K. (1978) Implementing a Real Time Computation and Display Algorithm for the Selspot System. S. M. Thesis, Department of Electrical Engineering, Massachusetts Institute of Technology.

Viviani, P. and Terzuolo, C. (1982) Trajectory determines movement dynamics. Neurosci. 7: 431-437.

8. Appendices

8.1. Appendix A

The change of movement dynamics with uniform speed scaling by a factor c was presented in (Hollerbach, 1984), but for reference is rederived below. Let $\underline{\theta}(t) = (\theta_1(t), \theta_2(t), \ldots, \theta_n(t))$ represent the time-varying n-dimensional vector of joint angles and $\underline{\tau}(t) = (\tau_1(t), \tau_2(t), \ldots, \tau_n(t))$ the corresponding time-varying vector of joint torques. A new trajectory $\tilde{\underline{\theta}}(t) = \underline{\theta}(ct)$ is defined that compresses or expands the time axis uniformly by a factor c. If $c > 1$ the movement is sped up; if $c < 1$ the movement is slowed down. The joint velocities and accelerations are related to the old as follows.

$$\dot{\tilde{\underline{\theta}}}(t) = c\dot{\underline{\theta}}(ct) \tag{A1}$$

$$\ddot{\tilde{\underline{\theta}}}(t) = c^2\ddot{\underline{\theta}}(ct) \tag{A2}$$

The movement dynamics can be compactly represented as

$$\underline{\tau}(t) = \mathbf{I}(\underline{\theta}(t))\ddot{\underline{\theta}}(t) + \dot{\underline{\theta}}(t) \cdot \mathbf{C}(\underline{\theta}(t)) \cdot \dot{\underline{\theta}}(t) + \mathbf{g}(\underline{\theta}(t)) \tag{A3}$$

where $\mathbf{I}(\underline{\theta}(t))$ is the $n \times n$ inertia matrix, $\mathbf{C}(\underline{\theta}(t))$ is the $n \times n \times n$ matrix of coriolis and centripetal coefficients, and $\mathbf{g}(\underline{\theta}(t))$ is the n-vector of gravity torques. The new torques $\tilde{\underline{\tau}}$ for the time-scaled movement are obtained by substituting (A1)-(A2) into (A3):

$$\tilde{\underline{\tau}}(t) = c^2\left[\mathbf{I}(\underline{\theta}(ct))\ddot{\underline{\theta}}(ct) + \dot{\underline{\theta}}(ct) \cdot \mathbf{C}(\underline{\theta}(ct)) \cdot \dot{\underline{\theta}}(ct)\right] + \mathbf{g}(\underline{\theta}(ct)) \tag{A4}$$

This expression can be more compactly represented by rewriting the dynamics in terms of drive torques $\underline{\tau}_{drive}$ and gravity torques $\underline{\tau}_{gravity}$.

$$\underline{\tau}(t) = \underline{\tau}_{drive}(t) + \underline{\tau}_{gravity}(t) \tag{A5}$$

where

$$\underline{\tau}_{drive}(t) = \mathbf{I}(\underline{\theta}(t))\ddot{\underline{\theta}}(t) + \dot{\underline{\theta}}(t) \cdot \mathbf{C}(\underline{\theta}(t)) \cdot \dot{\underline{\theta}}(t) \tag{A6}$$

$$\underline{\tau}_{gravity}(t) = \mathbf{g}(\underline{\theta}(t)) \tag{A7}$$

Then (A4) becomes

$$\tilde{\underline{\tau}}(t) = c^2\underline{\tau}_{drive}(ct) + \underline{\tau}_{gravity}(ct) \tag{A8}$$

8.2. Appendix B

The change of movement dynamics with load is best demonstrated by combining the dynamics of the arm without a load with the dynamics of a massless phantom arm carrying the load. We consider here the dynamics of the massless arm driving the load. Due to its movement, the load exerts a force $\mathbf{f}$ and a torque $\mathbf{n}$ on the tip of the phantom arm given by the Newton-Euler equations:

$$\mathbf{f} = m\ddot{\mathbf{r}} \tag{B1}$$

$$\mathbf{n} = \mathbf{I}\dot{\underline{\omega}} + \underline{\omega} \times \mathbf{I}\underline{\omega} \tag{B2}$$

where m is the load mass, $\ddot{\mathbf{r}}$ is the acceleration of the load center of gravity, $\mathbf{I}$ is the inertia tensor of the load about the center of gravity, and $\underline{\omega}$ and $\dot{\underline{\omega}}$ represent the angular velocity and acceleration of the loads. Again, the gravity torques will be treated separately later.

How can we turn forces and torques at the tip of the phantom arm into joint torques? Let $\mathbf{x} = (x_1, x_2, \ldots, x_m)$ represent the m-dimensional position and orientation vector that locates the load in space. Then the load trajectory is related to the joint trajectory by the vector function $\mathbf{h} = (h_1, h_2, \ldots, h_m)$ where

$$\mathbf{x} = \mathbf{h}(\underline{\theta}) \tag{B3}$$

Differentiating,

$$\dot{\mathbf{x}} = \mathbf{J}\dot{\underline{\theta}} \tag{B4}$$

where elements of the Jacobian matrix J are given by

$$J_{ij} = \frac{\partial h_i(\underline{\theta})}{\partial \theta_j} \tag{B5}$$

By the principle of virtual work (Brady, Hollerbach, Johnson, Lozano-Perez, and Mason, 1982),

$$\underline{\tau}^T_{drive}\dot{\underline{\theta}} = [\mathbf{f}^T \mathbf{n}^T]\dot{\mathbf{x}} \tag{B6}$$

where $\underline{\tau}^T_{drive}$ is the drive torque for the phantom arm. Substituting from (B4) and transposing, it can be seen that

$$\underline{\tau}_{drive} = \mathbf{J}^T \begin{bmatrix} \mathbf{f} \\ \mathbf{n} \end{bmatrix} \tag{B7}$$

We have found the torques necessary to drive the phantom arm with the load at the tip. We calculate the torques necessary to hold the load up against the force of gravity in the same way

$$\underline{\tau}_{gravity} = \mathbf{J}^T \begin{bmatrix} m\mathbf{g} \\ \mathbf{0} \end{bmatrix} \tag{B8}$$

where m is the mass of the object and $\mathbf{g}$ is the gravitational constant.

Suppose the load mass and moment of inertia scale by a factor r. Then the new mass $\tilde{m}$ and inertia $\tilde{\mathbf{I}}$ are linearly related to the old by

$$\tilde{m} = rm \tag{B9}$$

$$\tilde{\mathbf{I}} = r\mathbf{I} \tag{B10}$$

The inertia scaling is a restrictive assumption that is not generally true, since a non-uniform change in load shape or density would change the inertia tensor in a more complex manner.

The assumption of linear inertia scaling is the simplest case, and may suggest experiments which are discussed in the main text. Then the new load force and torque is obtained form the Newton-Euler equations as

$$\tilde{\mathbf{f}} = r\,\mathbf{f} \tag{B11}$$

$$\tilde{\mathbf{n}} = r\,\mathbf{n} \tag{B12}$$

Note that if the moment of inertia did not scale linearly, then the load force and torque would change differently. The new drive torques for the phantom arm are obtained from (B7) and (B11)-(B12):

$$\tilde{\mathcal{I}}_{drive} = r\,\mathcal{I}_{drive} \tag{B13}$$

The gravity torques for the phantom arm scale by r as well since they are proportional to the load mass.

$$\tilde{\mathcal{I}}_{gravity} = r\,\mathcal{I}_{gravity} \tag{B14}$$

Combining (B13) and (B14), the load-scaled total phantom arm torques are

$$\tilde{\mathcal{I}} = r\,\mathcal{I}_{drive} + r\,\mathcal{I}_{gravity} \tag{B15}$$

When speed scaling of the phantom arm is considered as well, the drive and gravity torques for the phantom arm scale differently. From (B1)-(B2), the net force and torque scale by c^2, hence the drive torques scale by c^2 from (B7), while again the gravity torques are speed independent.

$$\tilde{\mathcal{I}} = c^2\,r\,\mathcal{I}_{drive} + r\,\mathcal{I}_{gravity} \tag{B16}$$

The joint torques of the phantom arm driving the load are simply added to the joint torques necessary to drive the arm with no load along the same trajectory by the principle of superposition.